Unsupervised Classification of Multifrequency and Fully Polarimetric SAR Images Based on the H/A/Alpha–Wishart Classifier

Laurent Ferro-Famil, Eric Pottier, *Member, IEEE,* and Jong-Sen Lee, *Fellow, IEEE*

***Abstract*—In this paper, we introduce a new classification scheme for dual frequency polarimetric SAR data sets. A (6×6) polarimetric coherency matrix is defined to simultaneously take into account the full polarimetric information from both images. This matrix is composed of the two coherency matrices and their cross-correlation. A decomposition theorem is applied to both images to obtain 64 initial clusters based on their scattering characteristics. The data sets are then classified by an iterative algorithm based on a complex Wishart density function of the 6×6 matrix. A class number reduction technique is then applied on the 64 resulting clusters to improve the efficiency of the interpretation and representation of each class. An alternative technique is also proposed which introduces the polarimetric cross-correlation information to refine the results of classification to a small number of clusters using the conditional probability of the cross-correlation matrix. These classification schemes are applied to full polarimetric P, L, and C-band SAR images of the Nezer Forest, France, acquired by the NASA/JPL AIRSAR Sensor in 1989.**

***Index Terms*—Multivariate statistics, radar polarimetry, synthetic aperture radar (SAR), terrain classification.**

I. Introduction

THE backscattering properties of a natural medium vary with the observation frequency according to its physical features, such as its structure or its size with respect to the radar wavelength. The scattering mechanism may remain almost unchanged for bare soil observation at L and C-bands, but may show a totally different aspect for forest remote sensing at P and C-bands. Incident waves with different wavelengths interact with different parts of a complex medium. The purpose of multifrequency analysis is to gather adequate information from each data set.

Many algorithms have been developed to classify natural media using polarimetric synthetic aperture radar (POLSAR) data [1]–[5]. Several approaches were derived to directly relate some basic characteristics of the targets to elements of the polarimetric covariance matrix [6]–[8]. More recently, polarimetric decomposition theorems were introduced in order to investigate the intrinsic physical properties of a natural medium by evaluating the underlying scattering mechanisms [9]–[12]. All these approaches realize an interpretation of the polarization of the backscattered wave and establish a relation between the medium physical properties and polarimetric transformations.

The use of multifrequency polarimetric data sets has shown to increase the interpretation capabilities of quantitative remote sensing of natural media [13], [14]. Some multifrequency fully polarimetric classification approaches were developed using various types of algorithms and techniques based on neural networks, fuzzy iterative classifiers, statistical segmentation, etc. [15]–[17]. Statistical classification using multivariate probability density functions (PDFs) permits us to define adaptive decision rules to segment data sets into more compact clusters in an unsupervised way. Moreover, a decision rule derived from a fully polarimetric representation leads to optimal results and provides information for class type identification by evaluating the underlying physical scattering mechanism [17].

Kong *et al.* [18] introduced a maximum likelihood (ML) decision rule based on the multivariate complex gaussian distribution of the elements of the coherent scattering matrix. In order to reduce the effects of speckle in polarimetric SAR images, data are generally processed through incoherent averaging and are represented by coherency matrices. Lee *et al.* [17] introduced the ML decision rule to the incoherent case by using the multivariate complex Wishart distribution of sample coherency matrices. A k-mean algorithm was applied to iteratively assign the pixels of the POLSAR image to one of the classes using the ML rule. Lee *et al.* [19] further improved the classification by using the H-α decomposition theorem [9] to provide an initial guess of the pixel distribution into the classes that produces a better convergence of the unsupervised classification algorithm.

In this paper, we propose an unsupervised classification of dual frequency POLSAR images by including the polarimetric information of both images. A (6×6) coherency matrix is constructed using the single look complex data from the two frequency images. This matrix includes the coherency matrices from each image as well as their cross-correlation [20], [21]. This matrix is shown to follow a Wishart distribution and a ML decision rule is derived. Similarly to the single image case, data sets are processed through a k-mean classifier after an initialization step consisting of applying the H-α classification procedure to each separate image. A class number reduction technique is then applied to the 64 resulting clusters to improve the efficiency of the interpretation and representation of each class' characteristics. An alternative approach is also proposed based on the introduction of the second image polarimetric information through the cross-correlation conditional statistics.

Manuscript received September 18, 2000; revised August 13, 2001.

L. Ferro-Famil and E. Pottier are with the Laboratoire Antennes Radar et Télécommunications, Université de Rennes 1, 35042 Rennes Cedex, France (e-mail: laurent.ferro-famil@univ-rennes1.fr; eric.pottier@univ-rennes1.fr).

J. S. Lee is with the Image Science Section, Remote Sensing Division, Naval Research Laboratory, Washington, DC 20375-5351 USA (e-mail: lee@ccf.nrl.navy.mil).

Publisher Item Identifier S 0196-2892(01)09890-4.

This procedure permits an efficient handling of the classification information by refining an initial classified data set with a small number of clusters and iteratively creating new classes. The probability density of a sample cross-correlation matrix conditionally to the polarimetric information in one image is derived in order to calculate a distance measure. This distance is used to perform an unsupervised splitting of a dual image cluster into two subsets.

In Section II, single frequency POLSAR data statistics in both coherent and incoherent cases are described. Section III is devoted to the derivations of dual-frequency POLSAR data statistics. The PDF of a dual-frequency (6×6) coherency matrix is introduced. This result is used to derive the gaussian conditional PDF of the cross-correlation matrix. Section IV contains unsupervised classification results obtained with single frequency images. In Section V, we introduce two new dual frequency data unsupervised classification schemes. The first classification technique relies on a ML distance derived from the Wishart PDF of the dual frequency (6×6) coherency matrix. The second classification scheme uses the conditional gaussian PDF to merge the significant features from each POLSAR data set. These classification schemes are then applied to full polarimetric P, L and C-bands SAR images of the Nezer forest acquired by NASA /JPL AIRSAR sensor (1989).

The classification results obtained with the different segmentation schemes are analyzed in Section VI. Specific criteria are defined to investigate the correspondence between the segmented clusters distribution and the location of the different types of natural medium over the scene. These criteria are used to evaluate in a quantitative way the performance of the different classification procedures.

II. Single-Frequency Polarimetric SAR Data Statistics

For a given measurement configuration, a target is fully characterized by its coherent scattering matrix $\mathbf{S}$ relating the incident and scattered Jones vectors. In the general case, this matrix is composed of four complex variables and is given by

$$\mathbf{S} = \begin{bmatrix} S_{\mathrm{HH}} & S_{\mathrm{HV}} \\ S_{\mathrm{VH}} & S_{\mathrm{VV}} \end{bmatrix}. \tag{1}$$

Using a straightforward lexicographic ordering of the scattering matrix elements, a complex target vector is obtained

$$\mathbf{k} = [\, S_{\mathrm{HH}} \quad S_{\mathrm{HV}} \quad S_{\mathrm{VH}} \quad S_{\mathrm{VV}} \,]^T. \tag{2}$$

It has been verified that when the radar illuminates an area of random surface of many elementary scatterers, $\mathbf{k}$ can be modeled as having a multivariate complex gaussian PDF $N_C(\mathbf{0}, \mathbf{\Sigma})$ of the form [18], [22]

$$f_{\mathrm{k}}(\mathbf{k}) = \frac{\exp\left(-\mathbf{k}^{\dagger}\mathbf{\Sigma^{-1}}\mathbf{k}\right)}{\pi^4 |\mathbf{\Sigma}|}. \tag{3}$$

The operator $\dagger$ denotes the conjugate transpose $|\,|$ represents the determinant, and $\mathbf{\Sigma} = E(\mathbf{k}\mathbf{k}^{\dagger})$ is the covariance matrix of $\mathbf{k}$. Kong *et al.* [18] defined an ML classification procedure based on the density function (3). A vector $\mathbf{k}$ is assigned to the class X_m according to the following decision rule:

$$\begin{aligned} \mathbf{k} \in X_m \text{ if } & d(\mathbf{k}, X_m) \leq d(\mathbf{k}, X_j) \, \forall j \neq m \\ & \text{with} \\ & d(\mathbf{k}, X_m) = \mathbf{k}^{\dagger}\mathbf{\Sigma}_m^{-1}\mathbf{k} + \ln|\mathbf{\Sigma_m}| \\ & \qquad - \ln\left(p\left(X_m\right)\right) \end{aligned} \tag{4}$$

with $\mathbf{\Sigma_m}$ the feature covariance matrix of the class X_m.

Data sets are generally processed using incoherent averaging techniques of data compression and/or speckle reduction. Multilook data result from the averaging of independent single-look incoherent representations. The n-look sample covariance matrix is obtained from n independent target vectors $\mathbf{k_i}$ as follows:

$$\mathbf{Z} = \frac{1}{n}\sum\nolimits_{i=1}^{n} \mathbf{k_i}\mathbf{k_i}^{\dagger}. \tag{5}$$

It has been shown that assuming that the target vectors have a $N_C(\mathbf{0}, \mathbf{\Sigma})$ distribution, $\mathbf{Z}$ follows a complex Wishart PDF with n degrees of freedom, $W_C(n, \mathbf{\Sigma})$, defined by [22]

$$\begin{aligned} p(\mathbf{Z}) = & \frac{n^{qn}\,|\mathbf{Z}|^{n-q}\exp\left(-\mathrm{tr}\left(n\mathbf{\Sigma^{-1}}\mathbf{Z}\right)\right)}{\mathrm{K}(n,q)|\mathbf{\Sigma}|^n} \\ & \text{with} \\ \mathrm{K}(n,q) = & \pi^{q(q-1)/2}\prod\nolimits_{i=1}^{q}\Gamma(n-i+1) \end{aligned} \tag{6}$$

with $\Gamma()$ the gamma function and $\mathrm{tr}(\mathbf{\Sigma^{-1}}\mathbf{Z})$ the trace of $\mathbf{\Sigma^{-1}}\mathbf{Z}$. The variable q represents the number of elements of the target vector. Similar to the single-look case, a Bayes ML classification leads to the definition of a decision rule [17]. Considering that the *a priori* probabilities of classes are equal, a sample covariance matrix of a pixel of the SAR image is assigned to the class X_m if $d_1(\mathbf{Z}, X_m) \leq d_1(\mathbf{Z}, X_j)\ \forall j \neq m$, [17], with

$$d_1\left(\mathbf{Z}, X_m\right) = \ln|\mathbf{\Sigma_m}| + \mathrm{tr}\left(\mathbf{\Sigma_m}^{-1}\mathbf{Z}\right). \tag{7}$$

III. Dual-Frequency Polarimetric SAR Data Statistics

When dealing with dual frequency images, the polarimetric information contained in a resolution cell represents the fully polarimetric characteristics of both data sets.

A. Dual Polarimetric Representation

In the case of dual-frequency polarimetric data classification, it is important to simultaneously take into account the polarimetric information from both images

$$\mathbf{w} = \begin{bmatrix} \mathbf{k_1} \\ \mathbf{k_2} \end{bmatrix} \tag{8}$$

where $\mathbf{k_1}$ and $\mathbf{k_2}$ are the target vectors belonging to the different images. The vector $\mathbf{w}$ has the dimension $\mathbf{p = 2q}$. The $(p \times p)$ n-look covariance matrix $\mathbf{A}$ summarizes the joint information from both images and has the following structure:

$$\begin{aligned} \mathbf{A} = & \frac{1}{n}\sum\nolimits_{j=1}^{n} \mathbf{w_j}\mathbf{w_j}^{\dagger} = \begin{bmatrix} \mathbf{A_{11}} & \mathbf{A_{12}} \\ \mathbf{A_{21}} & \mathbf{A_{22}} \end{bmatrix}, \\ & \text{with} \\ \mathbf{A_{rs}} = & \frac{1}{n}\sum\nolimits_{j=1}^{n} \mathbf{k_{rj}}\mathbf{k_{sj}^{\dagger}}. \end{aligned} \tag{9}$$

The matrices $\mathbf{A_{11}} = \mathbf{Z_1}$ and $\mathbf{A_{22}} = \mathbf{Z_2}$ are the standard n-look $(q \times q)$ covariance matrices from separate images. $\mathbf{A_{12}} (= \mathbf{A_{21}^{\dagger}})$ is a $(q \times q)$ complex matrix containing information about the polarimetric cross-correlation between $\mathbf{k_1}$ and $\mathbf{k_2}$. The target vector $\mathbf{w}$ follows a complex normal distribution $N_C(\mathbf{0}, \mathbf{\Sigma_w})$ [22], with $\mathbf{\Sigma_w} = E(\mathbf{w}\mathbf{w}^{\dagger})$ its $(q \times q)$ covariance matrix. The sample $(p \times p)$ covariance matrix $\mathbf{A}$ has a complex Wishart distribution $W_C(n, \mathbf{\Sigma_w})$, characterized by n degrees of freedom

$$p(\mathbf{A}) = \frac{n^{pn} |\mathbf{A}|^{n-p} \exp\left(-n \operatorname{tr}\left(\mathbf{\Sigma_w^{-1}A}\right)\right)}{\mathrm{K}(n,p) |\mathbf{\Sigma_w}|^n} \tag{10}$$

with $\mathrm{K}(n,p)$ defined in (6). The advantage in using the $(p \times p)$ representation resides in the fact that according to (10), dual data sets can be simultaneously classified by using the ML distance measure defined in (11) and without any assumption concerning their independence

$$d_2(\mathbf{A}, \mathbf{X}_m) = \ln |\mathbf{\Sigma_{wm}}| + \operatorname{tr}\left(\mathbf{\Sigma_{wm}^{-1}A}\right) \tag{11}$$

with $\mathbf{\Sigma_{wm}}$ the $(p \times p)$ feature matrix of class X_m.

B. Cross-Correlation Matrix Statistics

The cross-correlation is highly sensitive to the scattering phenomenon type and its degree of randomness, both of which can be extracted from this covariance matrix representation. The probability of $\mathbf{A_{12}}$ may then be taken into account to separate groups of pixels belonging to the same class but possessing slightly different dual polarimetric information.

The properties of the hermitian matrix $\mathbf{A}$ permit to define a conditional probability of the polarimetric cross-correlation matrix $\mathbf{A_{12}}$. In order to express the conditional probability of $\mathbf{A_{12}}$ given $\mathbf{A_{22}}$, $p(\mathbf{A_{12}}|\mathbf{A_{22}})$, both $\mathbf{A}$ and $\mathbf{\Sigma_w}$ can be partitioned as follows [23]:

$$\mathbf{A} = \begin{bmatrix} \mathbf{A_{11.2}} + \mathbf{A_{12}A_{22}^{-1}A_{21}} & \mathbf{A_{12}} \\ \mathbf{A_{21}} & \mathbf{A_{22}} \end{bmatrix}$$
$$\mathbf{\Sigma_w} = \begin{bmatrix} \mathbf{\Sigma_{A11.2}} + \mathbf{\Sigma_{A12}\Sigma_{A22}^{-1}\Sigma_{A21}} & \mathbf{\Sigma_{A12}} \\ \mathbf{\Sigma_{A21}} & \mathbf{\Sigma_{A22}} \end{bmatrix} \tag{12}$$

with $\mathbf{A_{11.2}} = \mathbf{A_{11}} - \mathbf{A_{12}A_{22}^{-1}A_{21}}$ and $\mathbf{\Sigma_{A11.2}} = \mathbf{\Sigma_{A11}} - \mathbf{\Sigma_{A12}\Sigma_{A22}^{-1}\Sigma_{A21}}$. By means of an upper-triangular transformation, the determinants of the $(p \times p)$ matrices are then simplified to the following expressions:

$$|\mathbf{A}| = |\mathbf{A_{22}}|\,|\mathbf{A_{11.2}}|$$
and
$$|\mathbf{\Sigma_w}| = |\mathbf{\Sigma_{A22}}|\,|\mathbf{\Sigma_{A11.2}}|\,. \tag{13}$$

After some reductions and combinations, an expression of $\operatorname{tr}(\mathbf{\Sigma_w^{-1}A})$ is found as a function of $\mathbf{A_{11.2}}, \mathbf{A_{12}}$ and $\mathbf{A_{22}}$, with

$$\begin{aligned} \operatorname{tr}\left(\mathbf{\Sigma_A^{-1}A}\right) = &\operatorname{tr}\Big[\mathbf{\Sigma_{A_{11.2}}^{-1}}\left(\mathbf{A_{12}} - \mathbf{\Sigma_{A_{12}}\Sigma_{A_{22}}^{-1}A_{22}}\right) \\ &\cdot \mathbf{A_{22}^{-1}}\left(\mathbf{A_{12}} - \mathbf{\Sigma_{A_{12}}\Sigma_{A_{22}}^{-1}A_{22}}\right)^{\dagger}\Big] \\ &+ \operatorname{tr}\left[\mathbf{\Sigma_{A_{22}}^{-1}A_{22}}\right] \\ &+ \operatorname{tr}\left[\mathbf{\Sigma_{A_{11.2}}^{-1}A_{11.2}}\right]. \end{aligned} \tag{14}$$

Inserting (13) and (14) into the Wishart probability function of $\mathbf{A}$ in (10), it can be shown that

$$p(\mathbf{A}) = p(\mathbf{A_{11.2}}, \mathbf{A_{12}}, \mathbf{A_{22}}) = p\left(\mathbf{A_{11.2}}\right) p\left(\mathbf{A_{12}}, \mathbf{A_{22}}\right) \tag{15}$$

with

$$\begin{aligned} p(\mathbf{A_{11.2}}) = &\frac{n^{q(n-q)} |\mathbf{A_{11.2}}|^{(n-q-q)}}{\mathrm{K}(n-q,q) |\mathbf{\Sigma_{A_{11.2}}}|^{(n-q)}} \\ &\times \exp\left[-\operatorname{tr}\left(n\mathbf{\Sigma_{A_{11.2}}^{-1}A_{11.2}}\right)\right] \end{aligned} \tag{16}$$

and (17), shown at the bottom of the page.

From (15) and (16), it is found that the matrix $\mathbf{A_{11.2}}$ is independent of $\mathbf{A_{12}}$ and $\mathbf{A_{22}}$ and follows a complex Wishart PDF $W_C(n-q, \mathbf{\Sigma_{A_{11.2}}})$.

As the sample covariance matrix of the second image, $\mathbf{A_{22}}$ follows a complex Wishart density function with n degrees of freedom $W_C(n, \mathbf{\Sigma_{A_{22}}})$ and since $p(\mathbf{A_{12}}, \mathbf{A_{22}}) = p(\mathbf{A_{12}}|\mathbf{A_{22}})p(\mathbf{A_{22}})$, the conditional probability density of the polarimetric cross-correlation matrix $\mathbf{A_{12}}$ given $\mathbf{A_{22}}$ is a complex normal function, given by the last line of (17). This complex normal density function may be formulated as [23]

$$\begin{aligned} &p\left(\mathbf{A_{12}}|\,\mathbf{A_{22}}\right) = N_C\left(\mathbf{M_{A_{12}|A_{22}}}, \mathbf{\Sigma_{A_{12}|A_{22}}}\right), \text{ with} \\ &\mathbf{M_{A_{12}|A_{22}}} = \mathbf{\Sigma_{A_{12}}\Sigma_{A_{22}}^{-1}A_{22}} \text{ and} \\ &\mathbf{\Sigma_{A_{12}|A_{22}}} = \mathbf{\Sigma_{A_{11.2}}} \otimes \mathbf{A_{22}} \Rightarrow \mathbf{\Sigma_{A_{12}|A_{22}}} = \mathbf{\Sigma_{A_{11.2}}^{T}} \otimes \mathbf{A_{22}} \end{aligned} \tag{18}$$

Equation (18) can be written under a conventional form using the properties of the Kroneker product $\otimes$, as shown in (19) at the bottom of the next page.

$\mathbf{y} = \operatorname{vec}(\mathbf{A_{12}^{\dagger}})$ is a q^2 complex element vector obtained by stacking the columns of $\mathbf{A_{12}^{\dagger}}$ under each other and $m = \operatorname{vec}(\mathbf{M_{A_{12}|A_{22}}^{\dagger}})$. This complex normal density function gives, for pixels belonging to the class X_m, the probability of the cross-correlation matrix conditionally to the second image sample covariance matrix. The logarithm of (19) is used to define a measure of the distance between the actual polarimetric cross-correlation $\mathbf{A_{12}}$ and its expected value when observing

$$\begin{aligned} p\left(\mathbf{A_{12}}, \mathbf{A_{22}}\right) = &\frac{n^{qn} |\mathbf{A_{22}}|^{(n-q)}}{\mathrm{K}(n,q) |\mathbf{\Sigma_{A_{22}}}|^n} \exp\left[-n \operatorname{tr}\left(\mathbf{\Sigma_{A_{22}}^{-1}A_{22}}\right)\right] \\ &\cdot \frac{n^{q^2} \exp\left[-n \operatorname{tr}\left(\mathbf{\Sigma_{A_{11.2}}^{-1}}\left(\mathbf{A_{12}} - \mathbf{\Sigma_{A_{12}}\Sigma_{A_{22}}^{-1}A_{22}}\right)\mathbf{A_{22}^{-1}}\left(\mathbf{A_{12}} - \mathbf{\Sigma_{A_{12}}\Sigma_{A_{22}}^{-1}A_{22}}\right)^{\dagger}\right)\right]}{\pi^{q^2} |\mathbf{\Sigma_{A_{11.2}}}|^q |\mathbf{A_{22}}|^q}. \end{aligned} \tag{17}$$

the second image polarimetric information $\mathbf{A_{22}}$ with

$$d_3(\mathbf{A_{12}}|\mathbf{A_{22}},\mathbf{X_m}) = n\,\mathrm{tr}\Big(\mathbf{\Sigma}_{\mathbf{A_{11.2}}}^{-1}(\mathbf{A_{12}}-\mathbf{M}_{\mathbf{A_{12}}|\mathbf{A_{22}}})\,\mathbf{A_{22}}^{-1} \times (\mathbf{A_{12}}-\mathbf{M}_{\mathbf{A_{12}}|\mathbf{A_{22}}})^{\dagger}\Big) + q\ln(|\mathbf{A_{22}}|). \quad (20)$$

IV. Single Image Classification Procedure

A. Classification Algorithm

For a reciprocal medium in a monostatic radar configuration, the target vector presented in (2) is modified as $\mathbf{k_P} = (1/\sqrt{2})[S_{\mathrm{HH}}+S_{\mathrm{VV}}\ S_{\mathrm{HH}}-S_{\mathrm{VV}}\ 2S_{\mathrm{HV}}]^T$, leading to the definition of the Pauli coherency matrix $\mathbf{T} = E(\mathbf{k_P}\mathbf{k_P}^{\dagger})$. The use of the coherency matrix instead of the lexicographic covariance matrix does not modify the density distribution types and the related equations defined previously [19].

The method used to perform a classification of a single image polarimetric data set is based on the use of an iterative k-mean algorithm and is described in details in [17], [19]. Four options have to be chosen by the user.

- The number of classes m.
- The initialization of the pixel distribution into the m classes.
- The distance measure from a pixel to the m class centers.
- The termination criterion.

The number of classes and the data assignment during the initialization step of the classification are critical points and determine the quality of the entire classification.

In [19], Lee *et al*. proposed to initialize the classes using the H-α classification scheme [9], [10], which provides eight classes relating to the underlying physical scattering mechanism. This splitting of the data set gives a stable initial approximation. The distance is estimated using the ML approach applied on the data statistics mentioned previously. The termination criterion may be selected from the estimation of the classification quality, when a maximum number of iterations is reached, or when a sufficiently low number of pixels are switching classes from one iteration to the next.

B. The H-α Classification Scheme

The n-look sample Pauli coherency matrix $\langle\mathbf{T}\rangle = (1/n)\sum_{i=1}^{n}\mathbf{k_P}\mathbf{k_P}^{\dagger}$ represents a distributed target with its rank greater than 1. $\langle\mathbf{T}\rangle$ cannot be related to a single scattering matrix $\mathbf{S}$ and must be decomposed in order to identify the global mean scattering mechanism.

Cloude and Pottier [19] introduced a polarimetric decomposition theorem based on the projection of the distributed coherency matrix onto its eigenvector basis. $\langle\mathbf{T}\rangle$ is decomposed into a weighted sum of three unitary matrices of rank one. Each represents a pure scattering mechanism

$$\langle\mathbf{T}\rangle = \sum_{i=1}^{3}\lambda_i\mathbf{v_i}\mathbf{v_i}^{\dagger} = \lambda_1\mathbf{T_1}+\lambda_2\mathbf{T_2}+\lambda_3\mathbf{T_3} \quad (21)$$

with λ_i the ith eigenvalue of $\langle\mathbf{T}\rangle$ and $\mathbf{v_i}$ its related eigenvector.

From this decomposition are extracted two meaningful roll-invariant parameters α and H [10].

- α stands for the indicator of the mean scattering mechanism. A value close to zero relates surface reflection for scattering from a dipole α equals $\pi/4$ and reaches $\pi/2$ when the target consists in a metallic dihedral scatterer.
- The entropy H is an indicator of the random behavior of the global scattering. Both H and α are strongly related to the observed scene geophysical properties and structure.

The unsupervised classification is achieved by projecting the pixels of an image onto the H-α plane which is segmented into eight regions. The interpretation of this segmentation can be found in [10]. The arbitrarily fixed linear decision boundaries may not fit the data distribution in the classification plane and cause inaccurate results by artificially merging two close types of targets like sea and smooth ground at L-band or splitting into different classes pixels belonging to a complex medium showing a distribution spread over one or several boundaries. Nonetheless this classification scheme provides an interpretation of the global scattering leading to an understanding of the relation between the response of a medium and its mean physical characteristics and can be used as a first guess of the different scattering types.

C. Application to POLSAR Data

The classification technique is applied on the Nezer site situated in the Landes Forest in the south-west of France. On August 16, 1989, full polarimetric data sets have been acquired by NASA JPL AIRSAR sensor at P, L and C-bands, with center frequencies at 0.44 GHz, 1.225 GHz and 5.3 GHz, respectively. The pixel spacing is 3 m $\times$ 6.6 m.

The scene contains bare soil areas and many homogeneous forested areas of maritime pines. Several tree-age groups are included from more than 41 years down to 5–8 years of age. Backscattering from the tree parcels is highly correlated to the age of the trees. Fig. 2 shows the span images of the Nezer site at P-band. Fig. 3 shows the results of the unsupervised Wishart classification applied on P-band and L-band POLSAR data sets. After four iterations, the results obtained using the unsupervised Wishart classifier depict an important improvement in the classification accuracy. The P-band classified image shows an interesting correspondence between the polarimetric classes and the

$$p(\mathbf{A_{12}}|\mathbf{A_{22}}) = p(\mathbf{y}|\mathbf{A_{22}}) = \frac{n^{q^2}\exp\left[-n(\mathbf{y}-\mathbf{m})^{\dagger}\left(\mathbf{\Sigma}_{\mathbf{A_{11.2}}}^{\mathbf{T}}\otimes\mathbf{A_{22}}\right)^{-1}(\mathbf{y}-\mathbf{m})\right]}{\pi^{q^2}\left|\mathbf{\Sigma}_{\mathbf{A_{11.2}}}^{\mathbf{T}}\right|^{q}|\mathbf{A_{22}}|^{q}}. \quad (19)$$

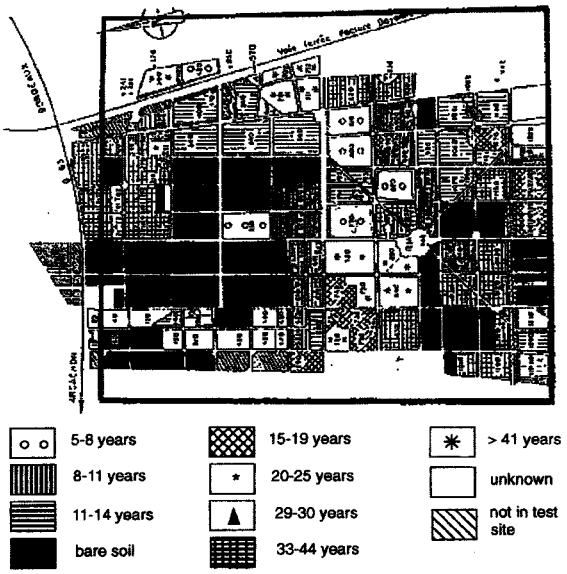

Fig. 1. Ground truth of Nezer Forest. This map is a courtesy of CESBIO and Dr. T. Le Toan.

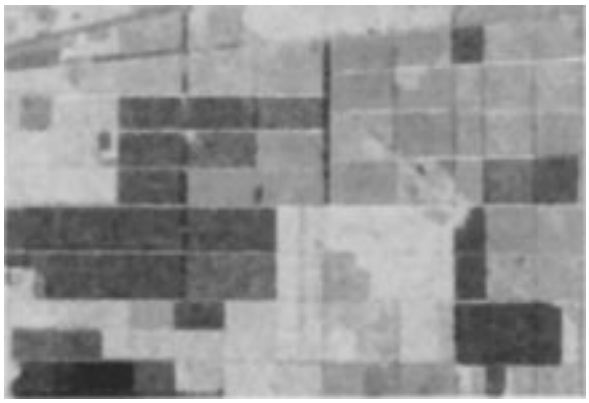

Fig. 2. Span image of the Nezer site at P-band.

ground-truth information. Class 5 represents the clear cut areas, whereas cells covered with 5–8 years old trees are occupied by class 8. Medium age trees, from 11 to 19 years old, are mainly covered by the polarimetric classes 4 and 7. Older tree cells, from 20 to more than 41 years old, have a polarimetric behavior corresponding to classes 1, 2, and 3. A polarimetric class may spread over more than one type of forest cell.

The L-band classified image does not separate different tree classes accurately. Young trees mainly correspond to class 4, while the rest of trees are represented by classes 1, 2, 3, 6, and 7. The unsupervised classification at this frequency highlights differences within the clear-cut regions, which are segmented in two different classes, 5 and 8.

This unsupervised classification algorithm modifies the decision boundaries in an adaptive way to better fit the natural distribution of the scattering mechanisms and takes into account the whole polarimetric information contained in the coherency matrix representation. The characterization and interpretation of the different clusters may be achieved by studying the polarimetric properties of their center feature matrix from the parameters delivered by the H-A-α decomposition or other full polarimetric analysis techniques [19], [24].

Fig. 3. Results for (top) P-band and (bottom) L-band data obtained with the unsupervised Wishart classifier.

V. Multifrequency Classification Procedure

We propose different approaches to the classification of several polarimetric data sets simultaneously. Dual frequency polarimetric images are classified by means of clustering procedures from the distance measure defined in (11) using the $(p \times p)$ coherency matrix representation, or successively (11) and (20) if the dual polarimetric information is introduced through the conditional probability density of the cross-correlation matrix.

A. Dual Frequency Image ML Classification

1) Classification Algorithm: Both of the separate images are classified through the unsupervised Wishart classifier into eight classes each. The results are further segmented into 64 classes by simultaneously considering the labels of pixels in each image. This way of initializing the pixel distribution presents the advantage of giving equal significance to the polarimetric information interpretation from each image.

The initial classified image, made of 64 clusters, is then processed through an unsupervised k-mean clustering algorithm based on the distance measure defined in (11). The use of the $(p \times p)$ dual polarimetric coherency matrix permits to calculate in an easy way the distance from a pixel to the different class center feature matrices. The dual image classification algorithm corresponding to the synopsis, described in Fig. 4, is the following.

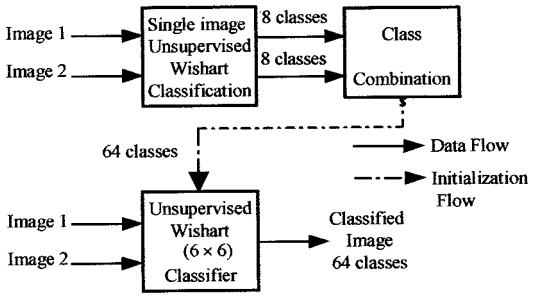

Fig. 4. Synopsis of an unsupervised dual frequency POLSAR image classification procedure.

Step 1: Perform the eight-class unsupervised Wishart classification on both separate polarimetric data sets.

Step 2: Initialize the class distribution by calculating the combined class number using the following rule: A pixel belonging to class X_{1i} in the first image and to X_{2j} in the second one is assigned to the combined class X_{i+8j}. The number of classes is then equal to 64.

Step 3: For each class X_i, compute the 6×6 feature covariance matrix $\mathbf{\Sigma_i} = (1/N_i)\sum_{N_i}\langle\mathbf{A}\rangle \in X_i$.

Step 4: Assign each pixel to the class minimizing the distance measure $d_2(\langle\mathbf{A}\rangle, X_m)$ from (11) over the 64 classes.

Step 5: Stop if a termination criterion is met, otherwise go to Step 3.

The accuracy, using this initialization, is highly enhanced, since pixels are distributed into 64 classes according to the combination of the full polarimetric unsupervised Wishart classification results obtained for separate images.

2) Reduction of the Number of Classes: The number of classes has to be reduced in order to facilitate the interpretation for each class characteristics as well as the visual representation of the geographical location of the different clusters. Lee *et al.* [19] proposed a merging procedure based on the study of the class compactness and separability that is well adapted to the natural partition of the data. Considering the entire class set, the clusters to be merged are the ones presenting the lowest degree of separability. Two classes can be distinguished, if they are compact and if the mean distance between their elements is high. Hence, the separability between classes X_i and X_j is defined as the ratio of their between-class distance to their within-class dispersion [19].

For a given class X_i, the within-class dispersion W_i is defined as the mean distance from its elements to the (6×6) class center feature matrix $\mathbf{\Sigma_i}$

$$W_i = \frac{1}{N_i}\sum\nolimits_{N_i} d_2\left[\left(\langle\mathbf{A}\rangle \in \mathbf{X_i}\right), \mathbf{X_i}\right]. \tag{22}$$

Inserting the definition of the distance measure of (11) in (22), one may find

$$W_i = \ln|\mathbf{\Sigma_i}| + \mathrm{tr}(\mathbf{I}) = \ln|\mathbf{\Sigma_i}| + z. \tag{23}$$

The constant term ($z = 6$) corresponds to the trace of the (6×6) identity matrix $\mathbf{I}$. The distance between class X_i and class X_j is the mean distance from the elements of each class to the center feature matrix of the other class. See equation (24), shown at the bottom of the next page.Using the definition of the distance measure, the average distance between two classes is simplified to

$$B_{ij} = \frac{W_i + W_j + \mathrm{tr}\left(\mathbf{\Sigma_i^{-1}\Sigma_j} + \mathbf{\Sigma_j^{-1}\Sigma_i}\right)}{2}. \tag{25}$$

Their separability $\mathrm{Sp}(X_i, X_j)$ is then given by

$$\mathrm{Sp}(X_i, X_j) = \frac{B_{ij}}{W_i + W_j}. \tag{26}$$

Using this definition and considering that the classes to be merged are those presenting the lowest separability, the class reduction technique is applied by the way of an iterative algorithm until a termination criterion is met.

One may use the termination introduced in [19] based on an estimation of the classification quality, or consider that the reduction procedure may end when an arbitrarily fixed number of classes is reached so that the classification results can be efficiently handled.

It is important to note the necessity of the intermediate classification step concerning the clustering of data in the six dimensional space. The merging of separately compact data sets may lead to diffuse classes in the higher dimension space. The (6×6) Wishart ML classification step permits to improve the compactness of the combined classes and significantly increases the efficiency of the class-number reduction procedure.

3) Application to POLSAR Data: The classification algorithm is run on P, L, and C-band data set combinations, with the number of classes reduced to 16. The classification results of P-band and L-band data sets are shown in Fig. 5. When comparing this classification method results with the ones obtained with a single image classification procedure, one finds an important improvement in the description of the natural characteristics distribution. The initialization step, which simultaneously takes into account both data sets with equal importance, produces a good discrimination of details like roads or lanes and small forest cells. The class number reduction technique permits to merge classes of close characteristics and produces an accurate distribution of the differently aged trees in the forest.

The classification map obtained from P and L-band images shows a good concordance with the parcel distribution given by the ground-truth information in Fig. 1. The relevant information from each data set has been gathered to differentiate the different

$$B_{ij} = \frac{\left(\frac{1}{N_i}\right)\sum_{N_i} d_2\left[\left(\langle\mathbf{A}\rangle \in X_i\right), X_j\right] + \left(\frac{1}{N_j}\right)\sum_{N_j} d_2\left[\left(\langle\mathbf{A}\rangle \in X_j\right), X_i\right]}{2}. \tag{24}$$

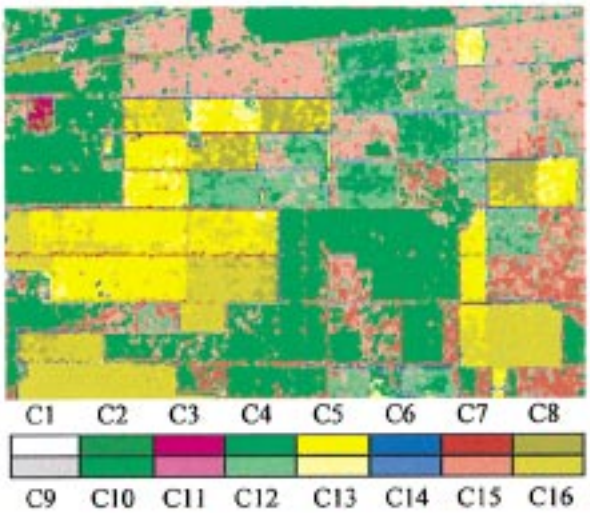

Fig. 5. Dual image unsupervised classification results obtained with P-L-band data sets.

parcel types. Globally, the P-band features permit to discriminate the different forest types, while L or C-bands characteristics emphasize the roads and lanes as well as the different types of bare ground areas. The compactness of the different classes is highly enhanced by this dual classification procedure.

It is important to note that no assumptions were made concerning the level of cross-correlation between the different data sets, the classification taking into account this information during the entire process.

B. Dual Frequency Image Classification Using the Cross-Correlation Information

1) Classification Algorithm: The procedure described above classifies data by reducing a high number of classes obtained by the combination of class labels in each image. The quality of classification depends on the accuracy of the separability criterion mentioned in (26). This top-down approach can be computationally intensive since it manipulates up to 64 classes.

A problem linked to the reduction of the number of classes may be encountered when classifying scenes composed of various types of scatterers. In the case of forest remote sensing, point targets or classes corresponding to heterogeneities may be considered as highly separable clusters, while the response of the different types of forest parcels may appear to be very close. During the class-number reduction process, the forest parcels may then be merged into classes containing a large number of pixels.

We propose another approach, which instead of initializing the classification with a high number of classes, begins with a small amount of classes and iteratively uses the conditional cross-correlation information to split one class into two subclasses. The synopsis of this classification scheme is presented in Fig. 6. The criterion used to choose the class to be split into two subclasses necessitates the calculation of the separability measure defined in (26). In each class the distance measure based on the cross-correlation information is calculated for each pixel from (20). The class X_m is temporarily split into two sub-classes X_{m1} and X_{m2} by comparing the value of the distance for each pixel with respect to the mean over the entire

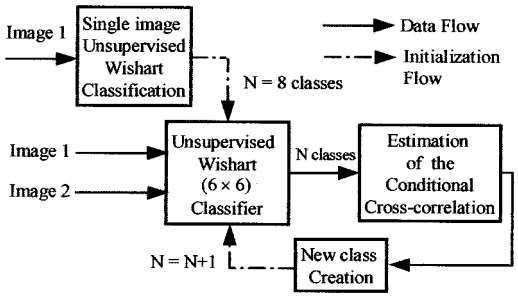

Fig. 6. Synopsis of an unsupervised dual frequency POLSAR image classification procedure using the polarimetric cross-correlation matrix conditional probability.

class equal to $\underline{d}_m = (1/N_m)\sum_{N_m} d_3(\mathbf{A_{12}}|\mathbf{A_{22}}, \mathbf{X}_m)$ for each $\mathbf{A} \in \mathbf{X_m}$.The decision rule is defined by

$$\text{For every } \mathbf{A} \in X_m, \text{ if } d_3\left(\mathbf{A_{12}}|\mathbf{A_{22}}, X_m\right) > \bar{d} \text{ then } \mathbf{A} \in X_{m1}, \text{ else } \mathbf{A} \in X_{m2} \tag{27}$$

The class to be split X_s is the one presenting the most distant subclasses and verifies

$$\text{Sp}(X_{s1}, X_{s2}) > \text{Sp}(X_{m1}, X_{m2})\ \forall s \neq m \tag{28}$$

where $\text{Sp}(X_{s1}, X_{s2})$ represents the separability between classes X_{s1} and X_{s2} and is defined in (26). The classification is initialized with the result of the single image based on the Wishart classification procedure. The number of classes is iteratively increased till a termination criterion is met.

The classification algorithm is defined as follows.

Step 1: Initialize the eight-class distribution from the unsupervised Wishart classification on one of the separate polarimetric data sets. The number of classes N is equal to eight.
Step 2: Apply the N-class unsupervised dual data sets Wishart classification using the (6×6) polarimetric representation, until a termination criterion is met.
Step 3: If a general termination criterion is met, go to Step 6.
Step 4: For each class, perform a temporary splitting into two subclasses, by applying the criterion defined in (27).
Step 5: Effectively split the class verifying (28) $N = N + 1$, go back to Step 2.
Step 6: Stop.

Similarly to the dual frequency image classification scheme, the general termination criterion may be obtained by evaluating the classification global quality from the parameter defined in [19], or by fixing a maximum number of classes. This procedure is less computationally intensive than the former one since the number of classes remains inferior or equal to the final one.

2) Application to POLSAR Data: The segmentation of P-L and P-C-band dual data sets in 16 clusters leads to almost similar results using both dual classification methods. The distribution of the classes is slightly different, but leads to an equivalent interpretation of the forest parcels. Due to the merging procedure,

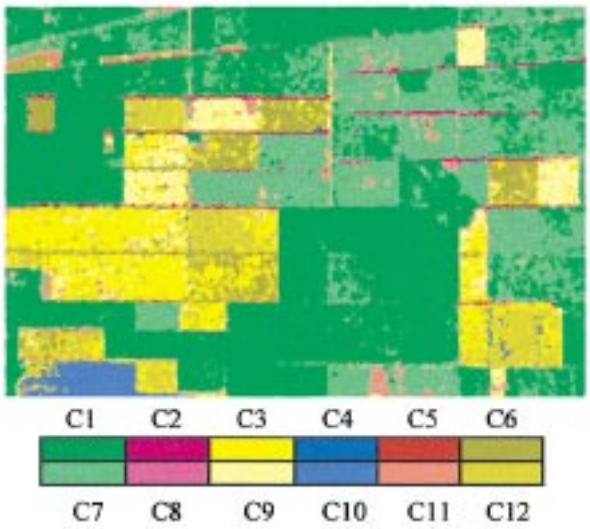

Fig. 7. Dual image unsupervised classification results obtained using P-C-band data sets with 12 classes.

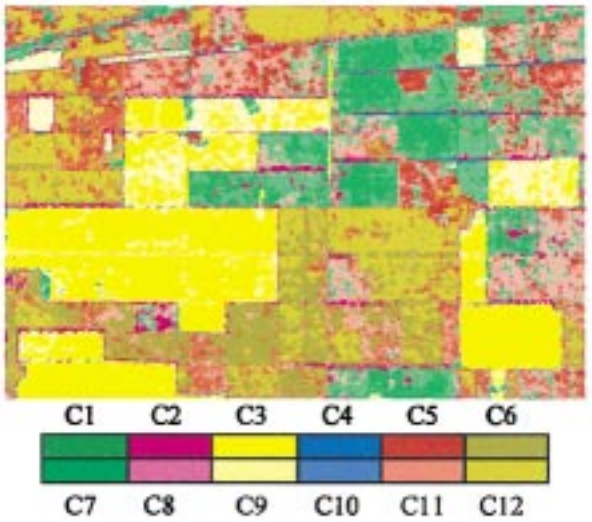

Fig. 8. Dual frequency image unsupervised classification results obtained with P-C-band data sets, using the cross-correlation matrix conditional probability, with 12 classes.

the classes produced by the first method are slightly more compact. We apply both classification methods to the dual P-C-band data set with a number of classes equal to 12.

The ML classification scheme provides a segmentation of the observed scene which gathers the almost totality of the tree covered parcels into two classes, classes number 1 and 7, as can be seen in Fig. 7.

During the class number reduction process, the polarimetric classes corresponding to the various types of forest show a low separability, compared to the point targets discriminated by C-band data and are merged into two classes so that the remaining clusters describe the bare soil areas. The joint use of these frequency bands with this classification method, using a small number of classes, does not provide good results for forest classification.

The classification based on the conditional probability of the cross-correlation matrix is initialized with eight clusters resulting from the Wishart iterative classification applied on one of the separate data sets and the class splitting procedure is run till the number of classes reaches 12. The classification results are shown in Fig. 8.

The classification provides better results than those depicted in Fig. 7 and provide good global information about the observed scene. The different types of forest parcels can be distinguished and the bare soil areas as well as the major part of the forest lanes are discriminated. This method is an efficient alternative to the ML dual classification, when the reduction procedure may merge close classes. An important gain in computation time was observed too.

As mentioned previously, the choice of the initial set of class center feature matrices has a significant influence on the classification performance. In a general way, the best classification results were obtained by initializing the process with the less spatially organized separately segmented data set. In our particular multifrequency forest remote sensing case, the degree of spatial disorder of the segmented data sets increases with the observation frequency. It is then recommended to initialize the classification with the highest center frequency data set. The class centers are then spread among a wide variety of scattering mechanisms. The more spatially organized information from the low center frequency data set permits to obtain compact final clusters.

VI. Analysis of the Classification Results

In order to evaluate the performance of the different classification schemes, some areas corresponding to six characteristic types of natural medium are selected in the SAR images as represented in Fig. 9. Zones I and II correspond to bare soil areas with different roughness scales. The areas with label III indicate parcels of young trees, while IV and V correspond to two types of intermediate age trees. The old tree stands are assigned to the type VI. The different areas have been chosen so as to contain approximately the same number of pixels.

The most representative polarimetric classes are associated, for each terrain type and in an exclusive way, in order to constitute the estimated population of the different given kinds of natural medium. The real population of each type of medium is given by the geographical location indicated in Fig. 9.The evaluation of the classification performance consists in the comparison, for each type of natural medium, of the estimated and real population, respectively, EP_i and RP_i.

The segmentation performance is investigated using three criteria aiming to evaluate the different clusters decriptivity, representativity and compactness.

The descriptivity D_i is defined as the percentage of pixels from the estimated population of a type of terrain effectively belonging to the real population of this kind of medium. It is formulated as follows:

$$D_i = \frac{\mathrm{EP}_i \in \mathrm{RP}_i}{\mathrm{EP}_i} \cdot 100. \tag{29}$$

The representativity of an estimated population R_i is calculated using the percentage of estimated populations from other types

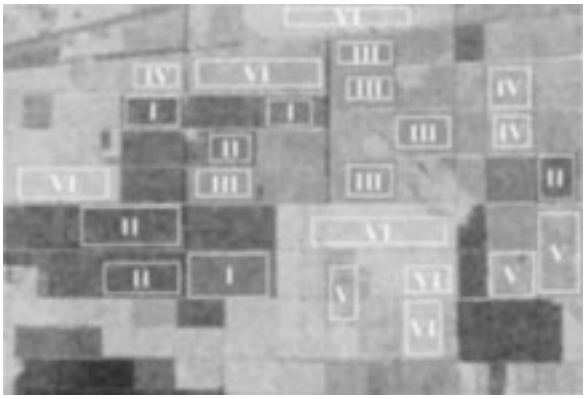

Fig. 9. Location of six types of natural medium over the Nezer forest scene.

of terrain EP_j, which also belong to the real population RP_i and are defined as

$$R_i = D_i - \sum_{j \neq i} \frac{\mathrm{EP}_j \in \mathrm{RP}_i}{\mathrm{EP}_i} \cdot 100 \text{ with } 0 \leq R_i \leq D_i. \quad (30)$$

If an estimated population is representative of a real population, R_i is close to D_i. On the other hand, when a large proportion of estimated populations from other types of terrain belongs to the real population, R_i tends to be equal to zero.

The last criterion concerns the compactness of an estimated population, C_i and can be calculated according to the following expression:

$$C_i = D_i - \sum_{j \neq i} \frac{\mathrm{EP}_i \in \mathrm{RP}_j}{\mathrm{EP}_i} \cdot 100 \text{ with } 0 \leq C_i \leq D_i. \quad (31)$$

When an estimated population is compact, C_i is close to D_i, while a large amount of pixels from an estimated population belonging to other types of terrain real populations makes C_i tend to be null. The different mono- and multifrequency classification method performance may be estimated from the criteria contained in Table I.

The numerical values of the descriptivity criteria are located on the diagonal of the subtables. Negative values for R_i an C_i are ignored.

The results of the single frequency data classification at L-band show the lowest descriptivity. Classifications at P, P-C, or P-L-bands present similarly high descriptivity values. It can be observed that classifications using a single frequency data set lead to clusters whose representativity and compactness are significantly lower than using dual frequency data. The additional information contained in a dual frequency data set permits to obtain clusters that better describe the different media distribution over the SAR image and then may lead to a more efficient and reliable interpretation for SAR data analysis and inversion.

VII. Conclusion

In this paper, we introduced a new unsupervised classification scheme for dual frequency polarimetric SAR data sets using a (6×6) polarimetric coherency matrix to simultaneously take into account the full polarimetric information from both images. Two classification methods were proposed. The first one was

TABLE I
CORRESPONDENCE OF THE ESTIMATED AND REAL POPULATIONS OF THE DIFFERENT TYPES OF TERRAIN

L band	RP1	RP2	RP3	RP4	RP5	RP6	C_i
EP1	**64.2**	35.7	0.8	0	0.8	0	**28.4**
EP2	10.6	**88.5**	0	0	0	0	**76.2**
EP3	0	0.2	**89.4**	10	89.4	0.3	**0**
EP4	0	0	23.7	**72.5**	23.7	3.6	**21.4**
EP5	0	1	56.3	42.1	**56.3**	0.5	**0**
EP6	0	0	2.6	58.7	2.6	**38.6**	**0**
D_i	**53.6**	**51.6**	**6**	**0**	**0**	**34.2**	

P band	RP1	RP2	RP3	RP4	RP5	RP6	C_i
EP1	**99.1**	99.1	2.8	0	0	0	**0**
EP2	97.1	**97.1**	0.8	0	0	0	**0**
EP3	0	0.	**75.8**	24.1	24.1	0	**27.5**
EP4	0	0	0.2	**87.9**	87.9	1.2	**0**
EP5	0	0	3	82.9	**82.9**	1.3	**0**
EP6	0	0	0	18	17.9	**72**	**36**
D_i	**2**	**0**	**69**	**0**	**0**	**69.5**	

P-C bands	RP1	RP2	RP3	RP4	RP5	RP6	C_i
EP1	**76**	23.8	0	0	0	0	**52.1**
EP2	8.1	**89.8**	0	0	0	0	**81.7**
EP3	0	0.	**94.4**	5.16	0	0	**89.1**
EP4	0	0	0.7	**65.9**	27.8	2.6	**34.8**
EP5	0	0	18.8	18.29	**59.4**	2.7	**19.6**
EP6	0	0	0	0.2	2.27	**97.3**	**94.7**
D_i	**67.9**	**66**	**74.9**	**42.3**	**29.3**	**92**	

P-L bands	RP1	RP2	RP3	RP4	RP5	RP6	C_i
EP1	**84**	15.7	0	0	0	0	**68.3**
EP2	8.5	**91.3**	0	0	0	0	**82.7**
EP3	0	0.	**98.2**	0	0.1	0	**97.8**
EP4	0	0	8.3	**85.9**	3	2.7	**71.9**
EP5	0	0	15	27.9	**47.3**	5.3	**0**
EP6	0	0	0	1	0.7	**98.3**	**96.6**
D_i	**75.5**	**75.6**	**74.9**	**57**	**43.5**	**90.3**	

based on an iterative algorithm using a ML decision rule evaluated from the Wishart density function of the (6×6) matrix. The initialization of this classification is realized a combination of the H-α classification results from each image providing 64 initial classes. Once the iterative algorithm has converged, a class number reduction technique is applied to improve the representation of each class characteristics. The results obtained with this classification show an important improvement in the description of the different types of natural media encountered in a forest scene. Parcels containing different types of trees can be distinguished and small classes such as roads and small forest parcels are discriminated. The class number reduction technique enhances the class compactness and improves the interpretation possibilities.

This reduction procedure may, in case of point targets, lead to the merging of large areas into a small number of polarimetric classes. In order to overcome this problem, a second technique was proposed, which introduces the polarimetric cross-correlation information and refines the results by iteratively creating new classes during the classification process. This method is an efficient alternative to the ML dual classification, when the reduction procedure may merge close classes and permits an important gain in computation time.

A quantitative analysis of the different classification scheme performance showed that the use of multifrequency data sets improved in a significant way the descriptivity, representativity and compactness of the segmentation results.

Since no assumptions were made concerning the nature of the data, the dual unsupervised classification approaches may be applied to any data sets acquired at different time, frequency or incidence angle without modification of the segmentation algorithms.

REFERENCES

[1] E. Rignot, R. Chellappa, and P. Dubois, "Unsupervised segmentation of polarimetric SAR data using the covariance matrix," *IEEE Trans. Geosci. Remote Sensing*, vol. 30, pp. 697–705, July 1992.

[2] H. A. Zebker, J. J. van Zyl, S. L. Durden, and L. Norikane, "Calibrated imaging radar polarimetry: Techniques examples and applications," *IEEE Trans. Geosci. Remote Sensing*, vol. 29, pp. 942–961, Nov. 1991.

[3] Hara, R. G. Atkins, S. H. Yueh, R. T. Shin, and J. A. Kong, "Application of neural networks to radar image classification," *IEEE Trans. Geosci. Remote Sensing*, vol. 32, pp. 100–110, Jan. 1994.

[4] J. J. van Zyl and C. F. Burnette, "Bayesian classification of polarimetric SAR images using adaptive a priori probabilities," *Int. J. Remote Sensing*, vol. 13, pp. 835–840, 1992.

[5] E. Pottier, "On full polarimetric target decomposition theorems with application to classification and identification of real target cross section," in *Proc. Int. Radar Conf.*, Paris, France, May 1994, pp. 330–335.

[6] J. J. van Zyl, "Unsupervised classification of scattering behavior using radar polarimetry data," *IEEE Trans. Geosci. Remote Sensing*, vol. 27, pp. 36–45, Jan. 1989.

[7] W. M. Boerner *et al.*, "Polarimetry in radar remote sensing: Basic and applied concepts," in *Principles and Applications of lmaging Radar, the Manual of Remote Sensing*, 3rd ed. New York: Amer. Soc. Photogramm. Remote Sensing, 1998, ch. 5.

[8] J. R. Huynen, "Phenomenological Theory of Radar Targets," Dr.Ing. dissertation, Drukkerij Bronder-offset, N.V. Rotterdam, Germany, 1970.

[9] S. R. Cloude and E. Pottier, "A review of target decomposition theorems in radar polarimetry," *IEEE Trans. Geosci. Remote Sensing*, vol. 34, pp. 498–518, Sept. 1995.

[10] ——, "An entropy based classification scheme for land applications of polarimetric SAR," *IEEE Trans. Geosci. Remote Sensing*, vol. 35, pp. 68–78, Jan. 1997.

[11] A. Freeman and S. Durden, "A three component scattering model to describe polarimetric SAR data," in *Radar Polarimetry*. New York: SPIE, 1992, vol. 1748, pp. 213–225.

[12] Y. Dong, B. Forster, and C. Ticehurst, "A new decomposition of radar polarization signatures," *IEEE Trans. Geosci. Remote Sensing*, vol. 36, pp. 933–939, May 1998.

[13] J. Shi and J. Dozier, "On estimation of snow water equivalence using Sir-C/X-SAR," in *Proc. 2nd Int. Workshop Retrieval of Bio- and Geo-Physical Parameters From SAR Data for Land Application*, Noordwijk, The Netherlands, Oct. 1998.

[14] D. M. Floricioiu, "Polarimetric Signatures and Classification of Alpine Terrain by Means of SIR-C/X-SAR," Ph.D. dissertation, Univ. Innsbruck, Innsbruck, Austria, 1997.

[15] K. S. Chen, W. P. Huang, D. H. Tsay, and F. Amar, "Classification of multi-frequency polarimetric SAR imagery using a dynamic learning neural network," *IEEE Trans. Geosci. Remote Sensing*, vol. 34, pp. 814–820, May 1996.

[16] A. Freeman, S. Durden, and R. Zimmerman, "Mapping sub-tropical vegetation using multi-frequency multi-polarization SAR data," in *Proc. IGARSS'92*, Houston, TX, June 1992, pp. 1686–1689.

[17] J. S. Lee, M. R. Grunes, and R. Kwok, "Classification of multi-look polarimetric SAR imagery based on the complex wishart distribution," *Int. J. Remote Sensing*, vol. 15, no. 11, pp. 2299–2311, 1994.

[18] J. A. Kong, S. H. Yueh, R. T. Shin, and J. J. van Zyl, "Classification of earth terrain using polarimetric synthetic aperture radar images," in *PIER*, J. A. Kong, Ed. Amsterdam, The Netherlands: Elsevier, 1990, vol. 3, ch. 6.

[19] J. S. Lee, M. R. Grunes, T. L. Ainsworth, L. Du, D. L. Schuler, and S. R. Cloude, "Unsupervised classification of polarimetric SAR images by applying target decomposition and complex wishart distribution," *IEEE Trans. Geosci. Remote Sensing*, vol. 37, pp. 2249–2258, Sept. 1999.

[20] S. R. Cloude and K. P. Papathanassiou, "Polarimetric SAR interferometry," *IEEE Trans. Geosci. Remote Sensing*, vol. 36, pp. 1551–1565, Sept. 1998.

[21] L. Ferro-Famil, E. Pottier, J. P. Dedieu, C. Corgier, and J. Saillard, "Application of polarimetric SAR data processing to snow cover remote sensing. Validation using optical images and ground data," in *Proc. Committee on Earth Observing Satellites SAR Workshop*, Toulouse, France, Oct. 26–29, 1999.

[22] N. R. Goodman, "Statistical analysis based on a certain multi-variate complex gaussian distribution (an introduction)," *Ann. Math. Statist.*, vol. 34, pp. 152–177, 1963.

[23] R. J. Muirhead, *Aspects of Multivariate Statistical Theory*. New York: Wiley, 1982.

[24] E. Pottier and J. S. Lee, "Application of the H/A/alpha polarimetric decomposition theorem for unsupervised classification of fully polarimetric SAR data based on the wishart distribution," in *Proc. Committee on Earth Observing Satellites SAR Workshop*, Toulouse, France, Oct. 26–29, 1999.

Laurent Ferro-Famil was born in Chateaurenard, France, in 1973. He received the electronics systems and computer engineering degree and the M.Sc. degree in electronics in 1996 and the Ph.D. degree in 2000, all from the University of Nantes, Nantes, France.

He is currently an Assistant Professor with the University of Rennes I, Rennes, France, in the Radar Polarimetry Group of the Antenna Radar Telecommunication (ART) Laboratory. His current activities in education are centered in the topics of analog electronics, microwave theory, and polarimetric radar imaging. He is especially interested in radar polarimetry theory and natural media polarimetric remote sensing with application to classification and electromagnetic scattering modeling and physical parameter inversion.

Eric Pottier (M'95) received the M.Sc. and Ph.D. degrees in signal processing and telecommunication from the University of Rennes 1, Rennes, France, in 1987 and 1990, respectively, and defended his Habilitation from the University of Nantes, Nantes, France, in 1998.

From 1988 to 1999, he was an Associate Professor at IRESTE-University of Nantes, where he was Head of the Polarimetry Group of the Electronic and Informatic Systems Laboratory. Since 1999, he has been a full Professor at the University of Rennes 1, where he is presently the Head of the Radar Polarimetry Group of the Antenna, Radar, and Telecommunication (ART) Laboratory. His current activities of research and education are centered in the topics of analog electronics, microwave theory, and radar imaging with emphasis in radar polarimetry. His research covers a wide spectrum of areas from radar image processing (SAR, ISAR), polarimetric scattering modeling, supervised/unsupervised polarimetric segmentation and classification to fundamentals, and basic theory of polarimetry. He is the Coordinator of the Quantitative Data Inversion Research Group of the European project Radar Polarimetry: Theory and Applications (TMR). He has supervised 25 research students to graduation (M.Sc. and Ph.D.) in radar polarimetry, covering areas from theory to remote sensing applications. He has chaired and organized 16 sessions in international conferences. He has been invited to present 19 presentations in international conferences and eleven in national conferences. He has five publications in books, 19 papers in refereed journals and more than 120 papers in conference and symposium proceedings.

Dr. Pottier was a member of the Organizing Committee of the first and second editions of the *International Workshop of Radar Polarimetry* in 1990 and 1992, the Scientific Co-Organizer (with Dr. S. R Cloude) of the third edition of this workshop in 1995, and the Scientific Chairman of the fourth edition in 1998. He was a member of the National Local Organizing Committee of the *Progress In Electromagnetic Symposium* (PIERS'98) of the Technical and Scientific Committees of European SAR 2000 (*EURSAR*) in 2000 and 2002, of the *Committee on Earth Observation Satellite SAR* (CEOS-SAR) Workshop in 1999 and 2001, and of the next Commission-F Triennium *Open Symposium on Radiowave Propagation and Remote Sensing* in 2002. He received the Best Paper Award during EUSAR2000 for his research activities, co-authored with J. S. Lee, Naval Research Laboratory, in the topic of polarimetric unsupervised segmentation of POLSAR data.

Jong-Sen Lee (S'66–M'69–SM'91–F'97) received the M.A. and Ph.D. from Harvard University Cambridge, MA, in 1965 and 1969, respectively.

Since then he has been with the U.S. Naval Research Laboratory (NRL), Washington DC, where he is presently the head of Image Science Section, Remote Sensing Division. He is also the principal investigator for several remote sensing programs on polarimetric SAR and interferometric SAR. He developed several speckle filtering algorithms that have been implemented in many GIS, such as ERDAS, PCI, ENVI, etc. His research covers a wide spectrum of areas from control theory, operation research and radiative transfer, to SAR and polarimetric SAR image processing. He has investigated SAR image segmentation, inverse SAR, polarimetric SAR imagery statistics and speckle filtering, SAR polarimetry, terrain/land-use classification and applications. His current research interests are in the area of SAR polarimetry, scattering signature modeling, Polarimetric SAR calibration, Polarimetric SAR interferometry and unsupervised segmentation and classification using polarimetric and interferometric SAR data.

Dr. Lee is a Fellow of IEEE for his contribution to information processing of SAR and polarimetric SAR imagery. He has chaired and organized many sessions in international conferences. He gave tutorials at IGARSS'97 and IGARSS'98. Currently, he is an associate editor of IEEE TRANSACTIONS ON GEOSCIENCE AND REMOTE SENSING. He has published more than 50 papers in refereed journals and more than 100 papers in conference proceedings.